ELECTROMECHANICAL SIMULATION OF ACTIVELY CONTROLLED ROTORDYNAMIC SYSTEMS WITH PIEZOELECTRIC ACTUATORS*

Reng Rong Lin and A.B. Palazzolo
Department of Mechanical Engineering
Texas A&M University
College Station, Texas 77843-3123, U.S.A.

A.F. Kascak
Propulsion Directorate
U.S. Army Aviation Systems Command
Lewis Research Center
Cleveland, Ohio 44135, U.S.A.

G. Montague
Sverdrup Technology, Inc.
Lewis Research Center Group
Brook Park, Ohio 44142, U.S.A.

This research developed theories and conducted tests for incorporating piezoelectric pushers as actuator devices for active vibration control. It started from a simple model with the assumption of ideal pusher characteristics and progressed to electro-mechanical models with non-ideal pushers. Effects on system stability due to the non-ideal characteristics of piezoelectric pushers and other elements in the control loop were investigated.

NOMENCLATURE

ADFT	Active damping feedback theory
ADSFT	Active damping and stiffness feedback theory
ASFT	Active stiffness feedback theory
AVC	: Active vibration control
$[C]$	: Damping matrix
C_i^A	: Feedback positive active damping
$[C_D]$	: Proportional damping matrix
C_{D_i}	: Capacitors used in differentiator
C_i	: Capacitors used in 2^{nd} order non-inverting LPF
C_s	: Damping coef. of the piezoelectric stack
e_1	: Eccentricity
$\{F_D(t)\}$	: External forces (disturbance)
F_{ix}	: Imbalance forces in x due to mass imbalance
F_{iy}	: Imbalance forces in y due to mass imbalance
F_{P_i}	: Force produced by the i^{th} pusher
F_j(S)	: J^{th} input of the transfer function
G_{ij}(S)	: Transfer function between the i^{th} output
	: the j^{th} input
K	: Feedback gain in amplifier
[K]	: Stiffness matrix
$[K^D]$	: Stiffness matrix including the pusher stiffness
$[K^{DD}]$	: Pusher stiffness matrix

*The authors gratefully acknowledge the funding for this research provided by NASA Lewis and the Texas A&M Turbomachinery Consortium. Sincere appreciation is also extended to the following people for their technical assistance: John Ropchock, Gerald Brown, and Tom Lakatos.

$[K_F]$: Feedback stiffness matrix
K_p : Preload spring inside the pusher
K_{PA} : Stiffness of pusher A
K_{PB} : Stiffness of pusher B
K_{RA} : Absorber stiffness at pusher A
K_{RB} : Absorber stiffness at pusher B
K_s : Stiffness of the stack of piezoelectric discs
LPF : Low pass filter
M : Number of actuators
[M] : Mass matrix
$[M_P]$: Lumped mass matrix of piezoelectric pushers
N : Number of degrees of freedom
R_{D_i} : Resistors used in differentiator
R_i : Resistors used in 2^{nd} order non-inverting LPF
R_F : Feedback resistor used in amplifier
R_I : resistor used in amplifier
T.F. : Transfer function
V_p : Probe voltage
Z_i^* : Pusher tip displacement
$\{\alpha\}$: Prescribed displacement of the pushers
β_i : scalar factors used in transfer function match
ζ_i : i^{th} modal damping
$[\Omega_i]$: i^{th} natural frequency

INTRODUCTION

There are two major strategies in rotordynamic vibration control: passive control and active control. Passive control is achieved by changing system parameters via passive damping components or devices. Some of these devices are Lanchester dampers, impact dampers, and squeeze-film dampers. Active control uses a servo-controller-actuator system to produce control forces which act directly upon the rotor in response to measured vibrations. Active vibration control has become an area of intense research in rotorbearing system dynamics. Research has been focused on developing effective active vibration control algorithms for machine tools, large space structures, and in robots. Significant efforts are being made to apply active vibration control (AVC) devices to rotating machinery in the petrochemical, aerospace and power utility industries. The advantages of active control over passive, i.e., absorbers and dampers, is the versatility of active control in adjusting to a myriad of load conditions and machinery configurations. This is clearly illustrated when one considers the very narrow bandwidth that a tuned spring mass absorber is effective in. Other advantages of AVC include compact size, light weight, and no lubrication systems needed in the control components, and the satisfactory operation in high or low temperature.

LITERATURE REVIEW

Electromagnetic shakers and magnetic bearings have been used for actuators in the majority of the active vibration control research mentioned in the literature. Magnetic bearings act directly onto the rotor without contact while electromagnetic actuators apply forces onto the rotor indirectly through the bearings. Schweitzer (1985) examined the stability and observability

of rotorbearing systems with active vibration control, and presented an analysis which related force and stiffness to electrical and geometrical properties of electromagnetic bearings.

Nikolajsen (1979) examined the application of magnetic dampers to a 3.2 meter simulated marine propulsion system. Gondhalekar and Holmes (1984) suggested that electromagnetic bearings be employed to shift critical speeds by altering the suspension stiffness. Weise (1985) discussed proportional, integral, derivative (PID) control of rotor vibrations and illustrated how magnetic bearings could be used to balance a rotor by forcing it to spin about its inertial axis. Humphris et al (1986) compared predicted and measured stiffness and damping coefficients for a magnetic journal bearing.

Several papers describe active vibration control utilizing other types of actuators such as pneumatic, hydraulic, electrohydraulic, and eddy current force generators. Ulbrich and Althaus (1989) discussed the advantages and disadvantages of different types of actutors, and examined controlled hydraulical chambers as force actuators. This compact system could develop very large forces and thereby influence even large turbines weighing several tons, however, the difficulty of hydraulic control lies in high frequency (over 100 Hz) response. This was essentially limited by the servo valve implemented and fluid losses. Feng (1986) developed an active vibration control scheme with actuator forces resulting from varying bearing oil pressure. Heinzmann (1980) employed loud speaker coils linked to the shaft via ball bearings to control vibrations.

Crawley and de L..is (1983, 1985) used piezoceramics, bonded on the surface of cantilever beams, as actuators either to excite vibrations or to suppress the vibrations by introducing damping to the system. Furthermore, they developed a theoretical background for predicting the amplitude of the vibration induced by piezoceramics. Stjernstrom (1987) bonded piezoceramics on cantilever beams as actuators and sensors to induce the 1^{st} and 2^{nd} vibration modes.

Matsubara et al (1989) employed piezoelectric dampers to suppress chatter vibration during a boring process. These piezoelectric dampers were driven so as to generate damping forces corresponding to the vibration velocity of the boring bar. Tzou (1987) demonstrated the control of bending vibration in non-rotating beams by using layered piezoelectric materials.

This paper considers the effects on the system stability due to the non-ideal characteristics of piezoelectric pushers and other control devices used in the control loop. The piezoelectric actuators are represented by equivalent, linear electric circuit with elements selected so as to match the frequency response function of the circuit to that of the actuator. The differential equations for the circuits are assembled into the structural matrices to form an electro-mechanical model of the system. This model may than be employed to predict instability onset feedback gains, total system stability and total system forced response.

ANALYSIS - GENERAL

The matrix differential equations of motion for a rotor bearing system can be derived by using Newton's 2^{nd} law or by Lagrange's method. Eq.(1) shows the matrix differential equation;

$$[M]_{(N\times N)}\{\ddot{Z}\}_{(N\times 1)} + [C]_{(N\times N)}\{\dot{Z}\}_{(N\times 1)} + [K]_{(N\times N)}\{Z\}_{(N\times 1)} = \{F(t)\}_{(N\times 1)} \qquad (1)$$

where [M], [C], and [K] matrices are the rotor bearing system mass, damping, and stiffness, respectively, N is the number of degrees of freedom, and $\{F\}$ represents the external forces exerted on the system.

Figure 1 (Palazzolo, 1981) shows a general rotor model with translatory and rotational dofs in the XZ and YZ planes. The model is discretized into lumped inertia stations which are connected by massless beam segments. The equilibrium equation of a disk is derived through the consideration of external forces present due to adjacent beam segments and the bearing stiffness forces.

The free vibration equilibrium equations for the entire rotor system are assembled by requiring internal equilibrium and displacement compatibility. Palazzolo (1981) shows how the [M], [K], and [C] matrices are formed for a generic rotorbearing system from basic geometric and material properties.

ANALYSIS - EQUIVALENT CIRCUITS

In previous references (Palazzolo, 1989) the free tip response of a piezoelectric pusher is assumed to be approximately equal to the internal prescribed displacement which is assumed to vary linearly with input voltage. These assumptions are valid only at frequencies well below the resonant frequency of the pusher. The phase lag of the piezoelectric pusher increases with frequency and may cause negative active damping to occur if the phase lag is greater than 90^0. Phase lag is also introduced by the pusher drivers and other electronic components in the control loop.

A linear time-invariant system with input $f(t)$ and with output $r(t)$ can be characterized by its impulse response $g(t)$, which is the response when subjected to an unit impulse input $\delta(t)$. Once the impulse response of the linear system is known, the output of the system $r(t)$, with any input $f(t)$, may be found from the transfer function of the system.

The transfer function of a linear time-invariant system is defined as the Laplace transform of the impulse response with zero initial conditions (Kuo, 1987). In general, if a linear system has p inputs and q outputs, the transfer function between the i^{th} output and the j^{th} input is defined as

$$G_{ij}(S) = \frac{R_i(S)}{F_j(S)} \tag{2}$$

where $F_k(S) = 0,\ k = 1, 2, \ldots, p,\ k \neq j.$

Equivalent electrical circuits are constructed to reproduce the measured transfer (frequency response) functions of the piezoelectric actuators and their amplifier drivers. These linear circuits may then be assembled with the structural system equations.

An electro-mechanical representation of an AVC system, consisting of a soft-mounted pusher, isolation pad, probe, and control devices, is shown in Figure 2. In this figure the buckout circuit removes DC bias from the eddy current displacement sensor, the low pass filter (L.P.F.) is utilized to reduce high frequency noise and improve stability. The figure also shows how the piezoelectric actuator and its amplifier driver are both represented by equivalent 2^{nd} order non-inverting low pass filters. With this model, the non-ideal characteristics of the overall system due to phase lag and frequency dependency can be included.

The differential equation for the differentiator in Figure 2 is

$$-\dot{V}_{in} = R_{D1}C_{D2}\ddot{V}_{out} + \left(\frac{R_{D1}}{R_{D2}} + \frac{C_{D2}}{C_{D1}}\right)\dot{V}_{out} + \frac{1}{R_{D2}C_{D1}}V_{out} \tag{3}$$

The corresponding transfer function is then

$$T.F. = \frac{V_{out}(S)}{V_{in}(S)} = \frac{-R_{D2}C_{D1}S}{\left[R_{D1}R_{D2}C_{D1}C_{D2}S^2 + \left(R_{D1}C_{D1} + R_{D2}C_{D2}\right)S + 1\right]} \tag{4}$$

If the variable 'S' in Eq.(4) is replaced by the variable 'jw', then Eq.(4) represents the frequency response function of the differentiator in the frequency domain.

The differential equation for the 2^{nd} order non-inverting low pass filter is

$$V_1 = \frac{R_1R_2C_1C_2}{K}\ddot{V}_2 + \left(-R_1C_1 + \frac{R_1C_2}{K} + \frac{R_1C_1}{K} + \frac{R_2C_2}{K}\right)\dot{V}_2 + \frac{1}{K}V_2 \tag{5}$$

The corresponding transfer function is then

$$T.F. = \frac{V_2(S)}{V_1(S)} = \frac{\frac{K}{(R_1R_2C_1C_2)}}{S^2 + \left[\frac{1}{C_1}\left(\frac{1}{R_1} + \frac{1}{R_2}\right) + \frac{1}{R_2C_2}(1-K)\right]S + \frac{1}{R_1R_2C_1C_2}} \tag{6}$$

Again, if the variable 'S' is replaced by the variable 'jw' in the above equation, Eq.(6) represents the frequency response function in the frequency domain and is shown below.

$$T.F. = \frac{V_2(jw)}{V_1(jw)} = \frac{K}{(1 - R_1R_2C_1C_2\omega^2) + jw[C_2(R_1 + R_2) + (1-k)R_1C_1]} \tag{7}$$

The electrically undamped natural frequency, ω_n, of this circuit is defined by

$$\omega_n^2 = \frac{1}{R_1R_2C_1C_2} \tag{8}$$

and the phase lag angle is

$$\phi = tan^{-1}\frac{\omega[C_2(R_1 + R_2) + (1-k)R_1C_1]}{1 - \left(\frac{\omega}{\omega_n}\right)} \tag{9}$$

The following steps summarize a simple procedure to identify the resistances and capacitances of an equivalent 2^{nd} order non-inverting low pass filter.

a) Make a frequency response plot of the physical system.
b) Locate the cut-off frequency, ω_n, from this plot.
c) Assume $R_1 = R_2$ and $C_1 = C_2$.

d) Select C_1 arbitrarily and then calculate R_1 by

$$R_1 = \frac{1}{\omega_n C_1}$$

e) Use $K = 3$ for an undamped electrical system and $K < 3$ for damped electrical system.
f) Construct the electrical circuit using the calculated R and C values.
g) Adjust the damping factor in the equivalent electrical circuit by varying the K value to match the peak magnitude at the cut-off frequency location.
h) Multiply this realized frequency response function by a proper scale factor which represents the magnitude ratio between the known and the realized frequency response functions at $\omega = 0$.

Figure 3 shows the schematic diagram for measuring the frequency response function of a pusher. The pusher is screwed inside a vertical steel cylinder and excited by a signal generator through the pusher driver. The displacement of the free tip of pusher, output for the transfer function, is measured by an eddy current probe. The exciting signal is the input for the transfer function. Both input and output are connected to a spectrum analyzer and the results of the transfer function are sent to a printer.

Figure 4 shows the transfer function of a typical pusher while Figure 5 shows the corresponding transfer function of the equivalent 2^{nd} order non-inverting low pass filter circuit with identified R and C values. This simulation shows a very good correlation between the two transfer functions when the frequency is below 4000 Hz. Note that a jet aircraft engine, depending on the size, normally operates at speeds from 5000 rpm (83.3 Hz) up to 25000 rpm (416.6 Hz). Furthermore, electro-mechanical instability frequencies have always occurred less than 4000 Hz, in our testing.

ANALYSIS - ELECTRO-MECHANICAL SYSTEM MODELING UTILIZING OPPOSING SOFT-MOUNTED ACTUATORS

The stability of the active vibration control system is affected by both the characteristics of the mechanical system (e.g. rotor) and those of the electrical devices (e.g. actuators) used in the control feedback loop. The characteristics, i.e. phase lag, of the electrical devices are incorporated in the mechanical system model by including their transfer function behavior represented by equivalent electrical circuits. Theory for the electro-mechanical model and comparisons between predicted and measured unbalance response and stability are presented.

Electro-Mechanical Model Theory

Let two opposing, soft-mounted pushers be installed at the j^{th} bearing of the rotor system (see Figure 6) where m_b, c_j, and k_j are the mass, damping, and stiffness of the j^{th} bearing, and k_{PA} and k_{PB} are the stiffnesses of pushers A and B and the dashed blocks represent the following components:

Block A: Inverting differentiator
Block B: 4^{th} order non-inverting low pass filter to simulate the Ithaco filter
Block C: 2^{nd} order non-inverting low pass filter to simulate pusher driver B
Block D: 2^{nd} order non-inverting low pass filter to simulate pusher B
Block E: 2^{nd} order non-inverting low pass filter to simulate pusher driver A

Block F: 2^{nd} order non-inverting low pass filter to simulate pusher A

Combining the mechanical and electrical differential equations for the model in Figure 6 yields

$$
\begin{pmatrix}
m_b & 0 & 0 & 0 & 0 & 0 & 0 & 0 & 0 & 0 \\
0 & m_{PA} & 0 & 0 & 0 & 0 & 0 & 0 & 0 & 0 \\
0 & 0 & m_{PB} & 0 & 0 & 0 & 0 & 0 & 0 & 0 \\
0 & 0 & 0 & R_{D1}C_{D2} & 0 & 0 & 0 & 0 & 0 & 0 \\
0 & 0 & 0 & 0 & 1 & 0 & 0 & 0 & 0 & 0 \\
0 & 0 & 0 & 0 & 0 & 1 & 0 & 0 & 0 & 0 \\
0 & 0 & 0 & 0 & 0 & 0 & 1 & 0 & 0 & 0 \\
0 & 0 & 0 & 0 & 0 & 0 & 0 & 1 & 0 & 0 \\
0 & 0 & 0 & 0 & 0 & 0 & 0 & 0 & 1 & 0 \\
0 & 0 & 0 & 0 & 0 & 0 & 0 & 0 & 0 & 1
\end{pmatrix}
\begin{pmatrix}
\ddot{x} \\ \ddot{x}_A \\ \ddot{x}_B \\ \ddot{V}_1 \\ \ddot{V}_2 \\ \ddot{V}_3 \\ \ddot{V}_4 \\ \ddot{V}_5 \\ \ddot{V}_6 \\ \ddot{V}_7
\end{pmatrix}
+
$$

$$
\begin{pmatrix}
c_j & 0 & 0 & 0 & 0 & 0 & 0 & 0 & 0 & 0 \\
0 & C_{RA} & 0 & 0 & 0 & 0 & 0 & 0 & 0 & 0 \\
0 & 0 & C_{RB} & 0 & 0 & 0 & 0 & 0 & 0 & 0 \\
\zeta_1 & 0 & 0 & \left(\frac{R_{D1}}{R_{D2}} + \frac{C_{D2}}{C_{D1}}\right) & 0 & 0 & 0 & 0 & 0 & 0 \\
0 & 0 & 0 & 0 & A_1 & 0 & 0 & 0 & 0 & 0 \\
0 & 0 & 0 & 0 & 0 & A_2 & 0 & 0 & 0 & 0 \\
0 & 0 & 0 & 0 & 0 & 0 & A_3 & 0 & 0 & 0 \\
0 & 0 & 0 & 0 & 0 & 0 & 0 & A_4 & 0 & 0 \\
0 & 0 & 0 & 0 & 0 & 0 & 0 & 0 & A_5 & 0 \\
0 & 0 & 0 & 0 & 0 & 0 & 0 & 0 & 0 & A_6
\end{pmatrix}
\begin{pmatrix}
\dot{x} \\ \dot{x}_A \\ \dot{x}_B \\ \dot{V}_1 \\ \dot{V}_2 \\ \dot{V}_3 \\ \dot{V}_4 \\ \dot{V}_5 \\ \dot{V}_6 \\ \dot{V}_7
\end{pmatrix}
+
$$

$$
\begin{pmatrix}
k_{11} & k_{12} & k_{13} & 0 & 0 & 0 & 0 & k_{18} & 0 & k_{110} \\
k_{21} & k_{22} & 0 & 0 & 0 & 0 & 0 & 0 & 0 & k_{210} \\
k_{31} & 0 & k_{33} & 0 & 0 & 0 & 0 & k_{38} & 0 & 0 \\
0 & 0 & 0 & k_{44} & 0 & 0 & 0 & 0 & 0 & 0 \\
0 & 0 & 0 & k_{45} & k_{55} & 0 & 0 & 0 & 0 & 0 \\
0 & 0 & 0 & 0 & k_{65} & k_{66} & 0 & 0 & 0 & 0 \\
k_{71} & 0 & 0 & 0 & 0 & k_{76} & k_{77} & 0 & 0 & 0 \\
0 & 0 & 0 & 0 & 0 & 0 & k_{87} & k_{88} & 0 & 0 \\
k_{91} & 0 & 0 & 0 & 0 & k_{96} & 0 & 0 & k_{99} & 0 \\
0 & 0 & 0 & 0 & 0 & 0 & 0 & 0 & k_{109} & k_{1010}
\end{pmatrix}
\begin{pmatrix}
x \\ x_A \\ x_B \\ V_1 \\ V_2 \\ V_3 \\ V_4 \\ V_5 \\ V_6 \\ V_7
\end{pmatrix}
=
\begin{pmatrix}
F(t) \\ 0 \\ 0 \\ 0 \\ 0 \\ 0 \\ 0 \\ 0 \\ 0 \\ 0
\end{pmatrix}
\tag{10}
$$

where

$k_{11} = k_j + k_{PA} + k_{PB}$ $\quad k_{12} = -k_{PA}$ $\quad k_{13} = -k_{PB}$

$k_{18} = k_{PB}\beta_7$ $\quad k_{110} = -k_{PA}\beta_8$

$k_{21} = -k_{PA}$ $\quad k_{22} = k_{RA} + k_{PA}$ $\quad k_{210} = k_{PA}\beta_8$

$k_{31} = -k_{PB}$ $\quad k_{33} = k_{RB} + k_{PB}$ $\quad k_{38} = -k_{PB}\beta_7$

$k_{44} = \frac{1}{C_{D1}R_{D2}}$

$k_{54} = -\omega_1^2 K_1 \beta_2$ $\quad k_{55} = \omega_1^2$

$k_{65} = -\omega_2^2 K_2$ $\quad k_{66} = \omega_2^2$

$$
\begin{aligned}
k_{71} &= \omega_3^2 K_3 \beta_1 \zeta_1 & k_{76} &= \omega_3^2 K_3 \beta_3 \beta_4 & k_{77} &= \omega_3^2 \\
k_{87} &= -\omega_4^2 K_4 \beta_5 & k_{88} &= \omega_4^2 & & \\
k_{91} &= -\omega_5^2 K_5 \beta_1 \zeta_1 & k_{96} &= -\omega_5^2 K_5 \beta_3 \beta_4 & k_{99} &= \omega_5^2 \\
k_{109} &= -\omega_6^2 K_6 \beta_6 & k_{1010} &= \omega_6^2 & &
\end{aligned}
\tag{11}
$$

and where K_i is the internal zero frequency gain of the individual filter and is defined as

$$
K_i = \frac{R_{I_i} + R_{F_i}}{R_{I_i}}, \qquad i = 1,2 \tag{12}
$$

and

$$
\omega_i^2 = \frac{1}{R_{2i-1} R_{2i} C_{2i-1} C_{2i}}, \qquad i = 1,2 \tag{13}
$$

$$
A_i = \left[\frac{1}{C_{2i-1}} \left(\frac{1}{R_{2i-1}} + \frac{1}{R_{2i}} \right) + \frac{1 - K_i}{R_{2i} C_{2i}} \right], \qquad i = 1,2 \tag{14}
$$

$$
\alpha_A = \beta_8 V_7 \tag{15}
$$

$$
\alpha_B = \beta_7 V_5 \tag{16}
$$

$$
V_p = \zeta_1 x \tag{17}
$$

Finally β_5 and $\hat{\beta}_7$ are the scale factors used to match the amplitudes of the transfer functions of the pusher driver B and pusher B, respectively.

The "electromechanical" element matrices in Eq.(10) are next assembled into the structural finite element model of the rotor bearing system described by Eq.(1). The total system model can then be employed for free or forced vibration response simulation.

TEST RESULT CORRELATION

Figure 7 shows a diagram of the actively controlled rotor bearing system at NASA Lewis. Each bearing has a control circuit as shown in this figure. Unbalance response was obtained by measuring the influence coefficients for an imbalance attached on the outboard disk. Figure 8 shows the measured influence coefficient at the outboard bearing for the controlled and uncontrolled cases. Figure 9 shows that the predicted influence coefficient as obtained from the electromechanical simulation model is in good agreement with the test results. The simulation model employed a proportional damping assumption for the uncontrolled (tare) system.

The Y_O velocity feedback gain was increased in Figure 7 until the system became unstable at zero rpm. The unstable mode shape was measured and appears in Figure 10. Figure 11 shows that the corresponding unstable mode predicted by the electromechanical simulation model is very similar in form and frequency. The instability onset-feedback gain was very sensitive to the amount of passive (uncontrolled) damping of the unstable mode. The measured passive damping ratios for this mode ranged between 0.0011 and 0.011. The measured instability onset feedback gain (β_4) was 5. The predicted value was 7 with a unstable mode passive damping of 0.0011. The utility of the simulation program as a design or trouble shooting tool for actively controlled

systems is demonstrated in Figure 12 which shows how stability can be controlled by changing resistance in the low pass filter.

Figure 13 shows the effectiveness of the control system in controlling two modes utilizing both active damping and stiffness.

SUMMARY

The authors have developed a new means for simulating the electromechanical response of rotorbearing system utilizing a piezoelectric actuator type active vibration control. The simulation results show good agreement with those measured on a two bearing turbine-driven test rig at NASA Lewis.

REFERENCES

[1] Crawley, E.F. and de Luis, J., 1983, "Experimental Verification of Piezoelectric Actuators for Use in Precision Space Structures," AIAA Paper 83-0878.

[2] Crawley, E.F. and de Luis, J., 1985, "Use of Piezoceramics as Distributed Actuators in Large Space Structures," Proceedings of the 26^{th} Structures, Structural Dynamics, and Materials Conference, Part 2, AIAA-ASME-ASCE, Orlando, Florida, April, pp. 126-133.

[3] Feng, G. Xin, N., 1986, "Automatic Control of the Vibration of the Flexible Rotor with Microcomputer," Int. Conf. on Rotordynamics, IFTOMM and JSME, Tokyo, Sept. pp.14-17.

[4] Gondholekar, V., and Holmes, R., 1984, "Design of Electromagnetic Bearing for Vibration Control of Flexible Transmission Shaft," Rotor Dynamic Instability Problem in High Performance Turbomachinery, Texas A&M Univ., May.

[5] Heinzmann, J.D., Flack, R., Lewis, D., 1980, "The Implementation of Automatic Vibration Control in High Speed Rotating Test Facility," Univ. of Virginia Report UVA/464761/MAE80/160.

[6] Hermann, E., 1988, Personal communications, Hartford Insurance, Houston, Texas

[7] Humphris, R., et al., 1986, "Effect of Control Algorithms on Magnetic Journal Bearing Properties," J. Eng. Gas Turbines and Power, ASME, Oct., Vol. 108, pp. 624-632.

[8] Matsubara, T., Yamamoto, H., Mizumoto, H., 1989, "Chatter Suppression by Using Piezoelectric Active Dampers," Rotatory Machinery Dynamics, DE-Vol. 18-1, 12^{th} Biennial Conference on Mechanical Vibration and Noise, Montreal, Quebec, Canada, September, pp. 79-83.

[9] Nikolajsen, J., Holmes, R. and Gondholekar, V., 1979, "Investigation of an Electromagnetic Damper for Vibration Control of a Transmission Shaft," Proc. Instn. Mech. Engr., Vol, 193, pp. 331-336.

[10] Palazzolo, A.B., 1981, "Vibrations of Locally Modified Mechanical and Structural Systems," University of Virginia Dissertation, Mechanical Engineering, January.

[11] Palazzolo, A.B., Lin, R.R., Kascak, A.F., Montague, J., Alexander, R.M., 1989, "Test and Theory for Piezoelectric Actuator - Active Vibration Control of Rotating Machinery,"

ASME Conf., Montreal, Canada, September, Submitted to the ASME Journal of Vibration, Acoustics, Stress, and Reliability in Design for publication.

[12] Palazzolo, A.B., Lin, R.R., Kascak, A.F., Montague, J., Alexander,R.M., 1989, "Piezoelectric Pushers for Active Vibration Control of Rotating Machinery," ASME Journal of Vibration, Acoustics, Stress, and Reliability in Design, Vol. 111, July, pp.298-305.

[13] Schweitzer, G., 1985, "Magnetic Bearings for Vibration Control," Bently Nevada Instability Seminar, Minden Nevada.

[14] Stjernstrom, Scott C., 1987, "Active Vibration Control Using Piezoceramic Transducers," Texas A&M University Thesis, Mechanical Engineering Department, December.

[15] Tzou, H.S., 1987, "Active Vibration Control of Flexible Structures Via Converse Piezoelectricity," Presented at the 20^{th} Midwestern Mechanics Conference, 8/31-9/2, 1987, Developments in Mechanics, pp.1201-1206, Vol. 14-c.

[16] Weise, D., 1985, "Active Magnetic Bearings Provide Closed Loop Servo Control for Enhanced Dynamic Response," Proc. 27^{th} IEEE Machine Tool Conf., October.

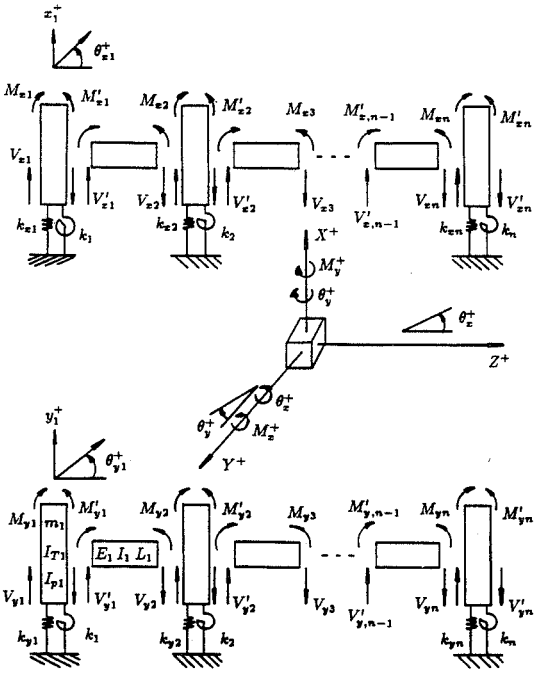

Figure 1 General n-disc rotor bearing system.

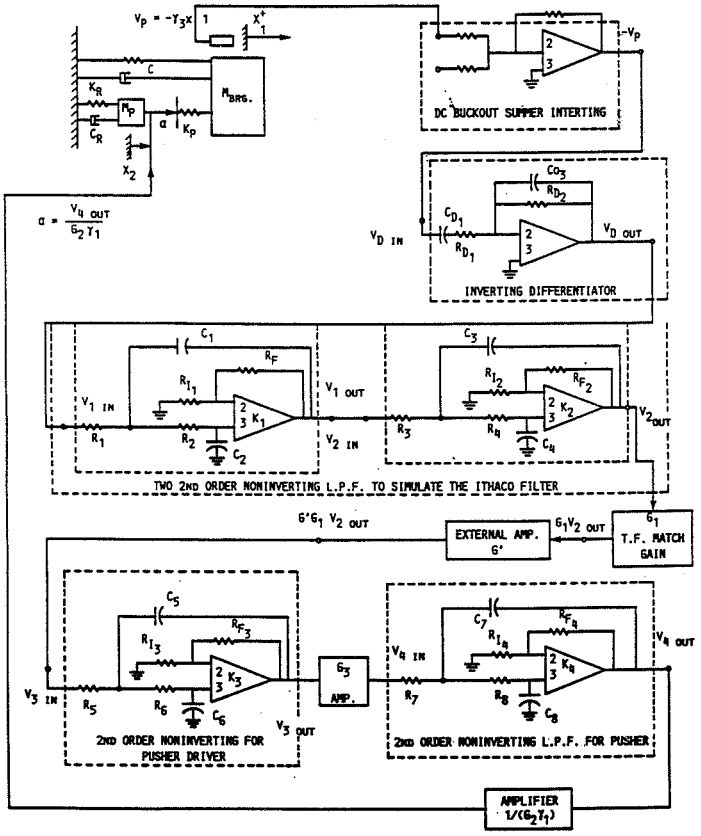

Figure 2 Soft-mounted single pusher with absorber.

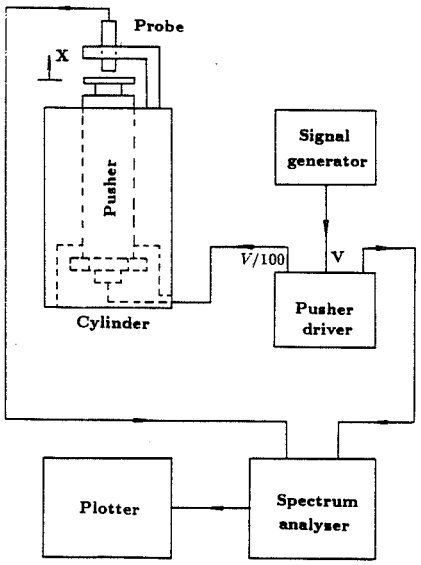

'Figure 3 Schematic diagram for measuring the pusher frequency response function.

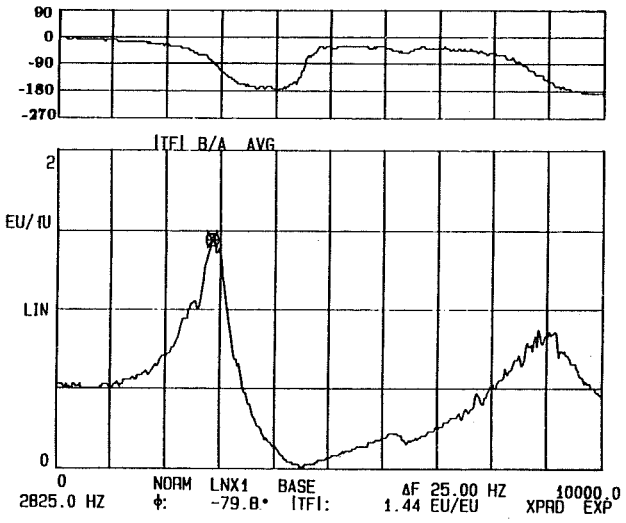

Figure 4 Transfer function plot of a typical pusher.

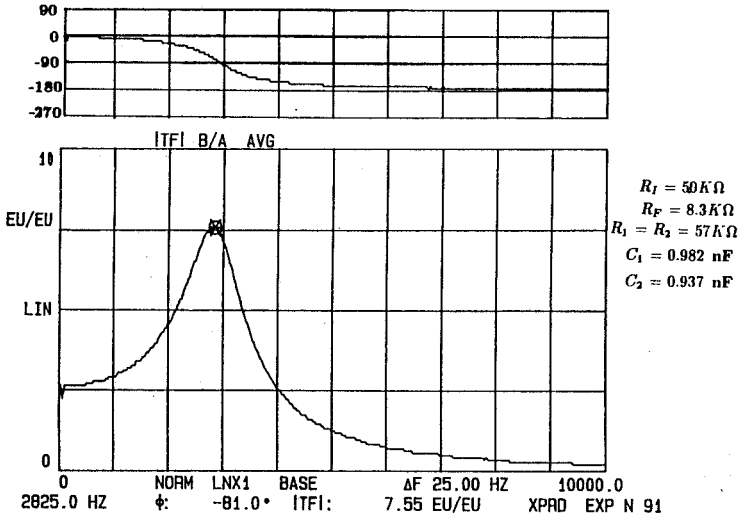

Figure 5 Transfer function plot of realized electrical circuit of pusher A.

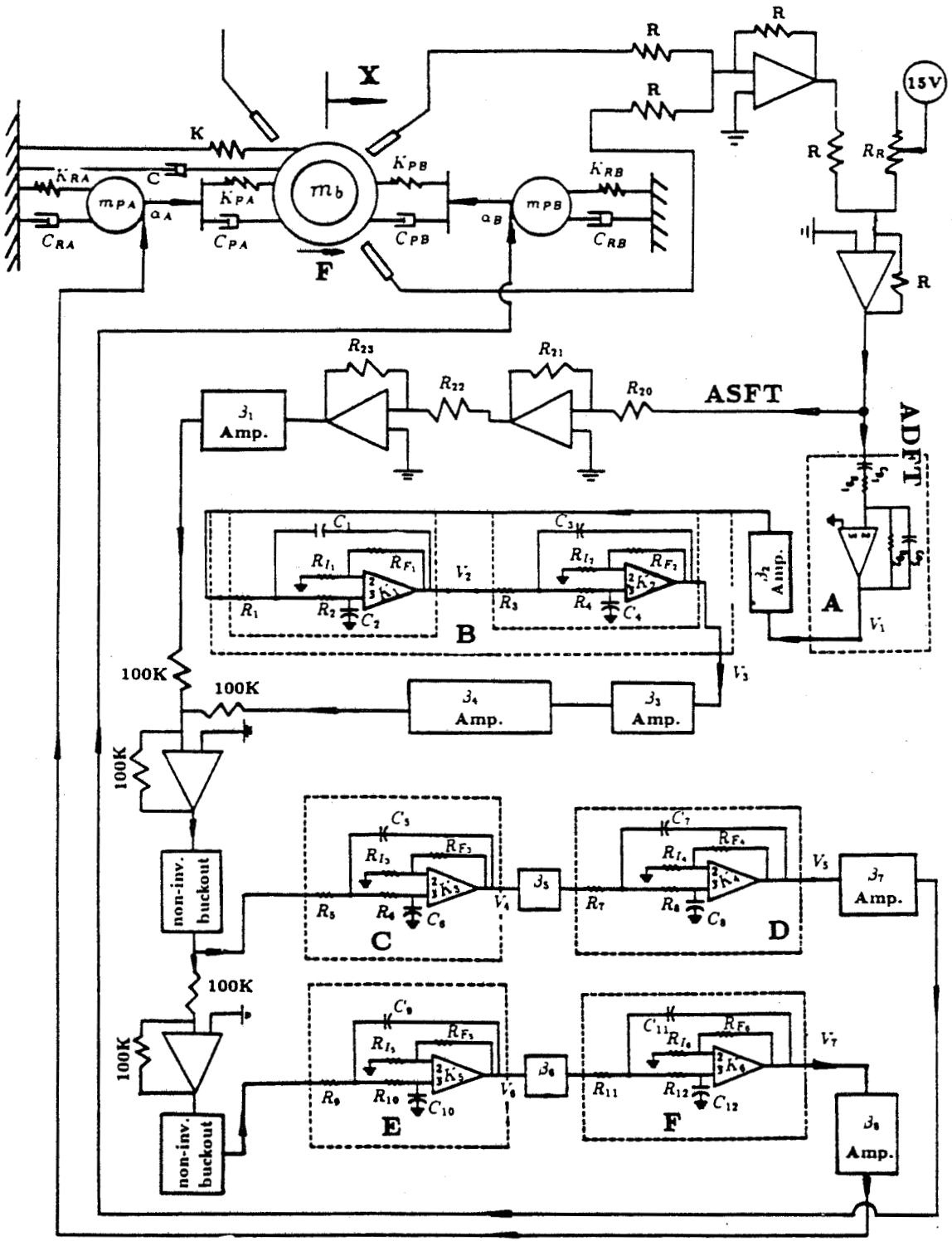

Figure 6 Electro-mechanical model with two opposing soft-mounted pushers.

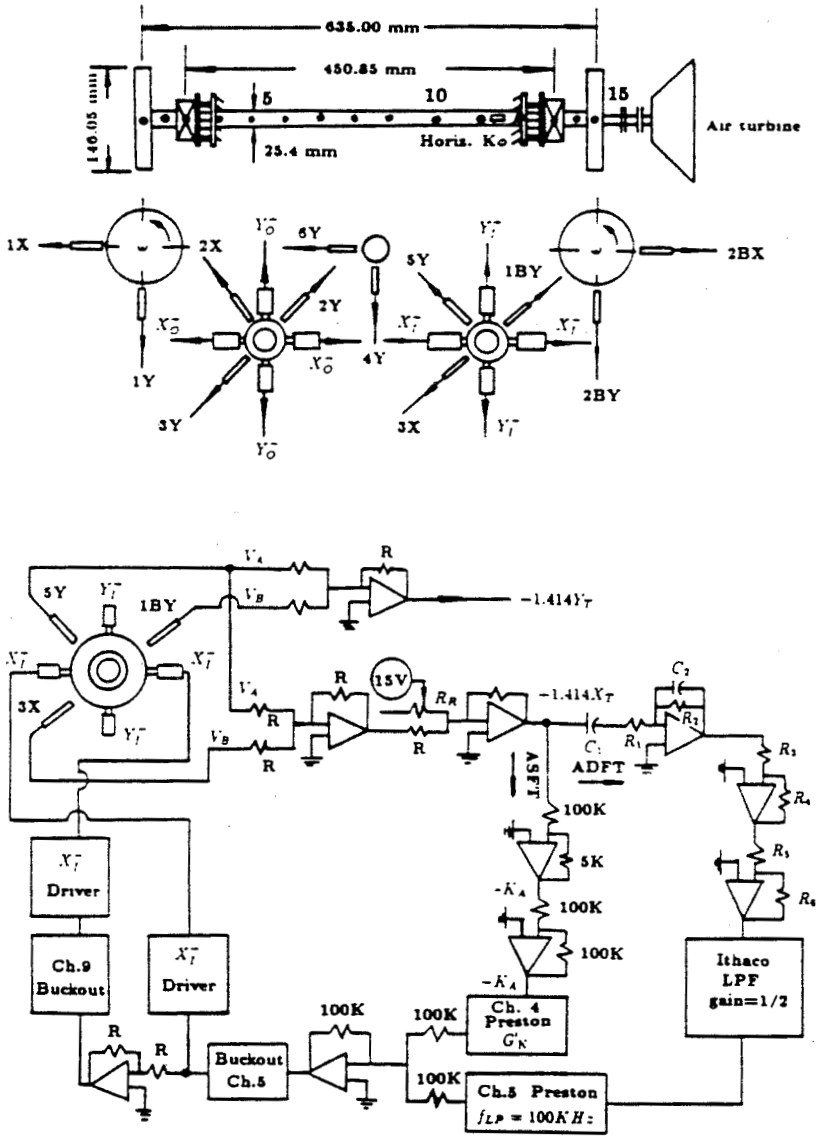

Figure 7 Schematic diagram of sensors, actuators, and control circuit of NASA test rig.

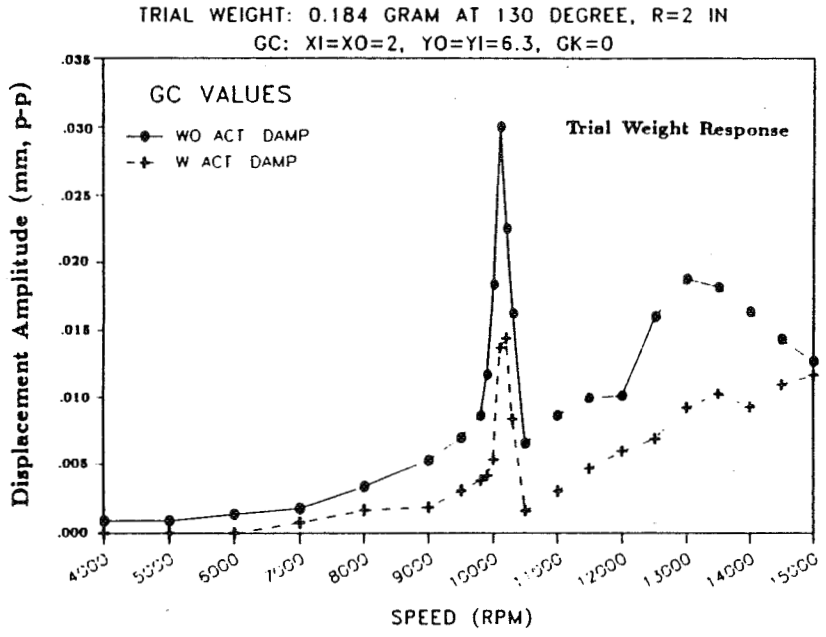

Figure 8 Measured unbalance responses at YO^{+}_{BRG} with and without ADFT.

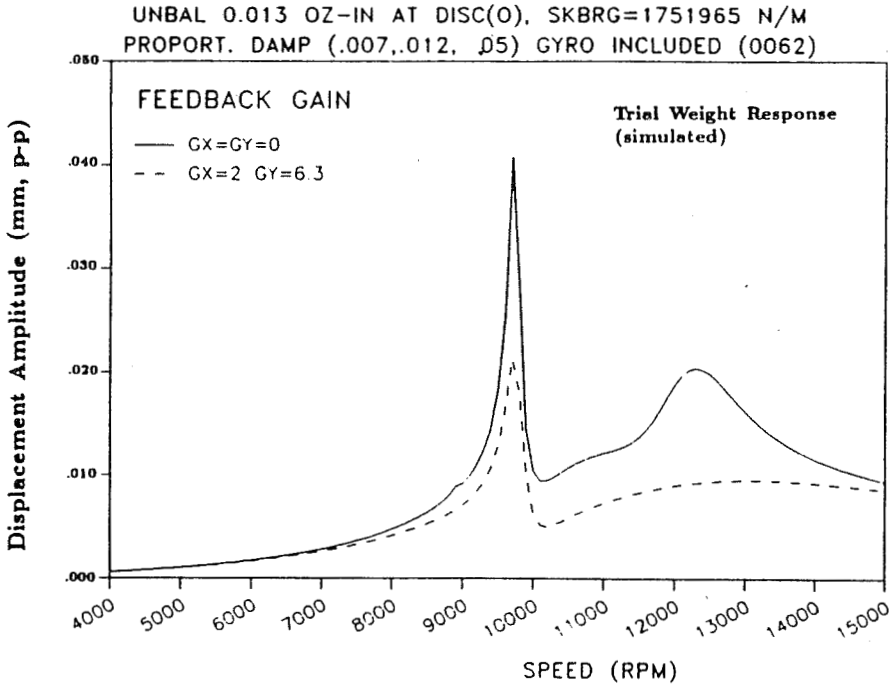

Figure 9 Simulated unbalance responses at YO^{+}_{BRG} with and without ADFT, with 3-mode proportional damping method.

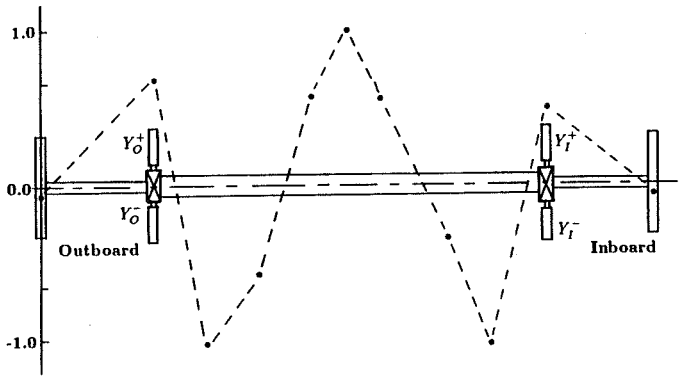

Figure 10 **Measured mode shape of unstable mode at a frequency of 2100 Hz.**

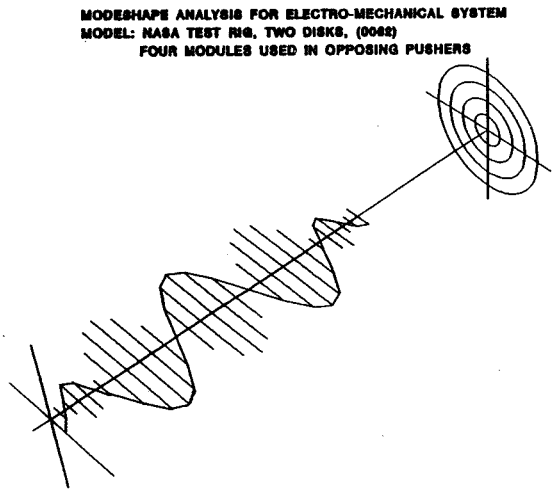

Figure 11 **Predicted mode shape of unstable mode at 2400 Hz.**

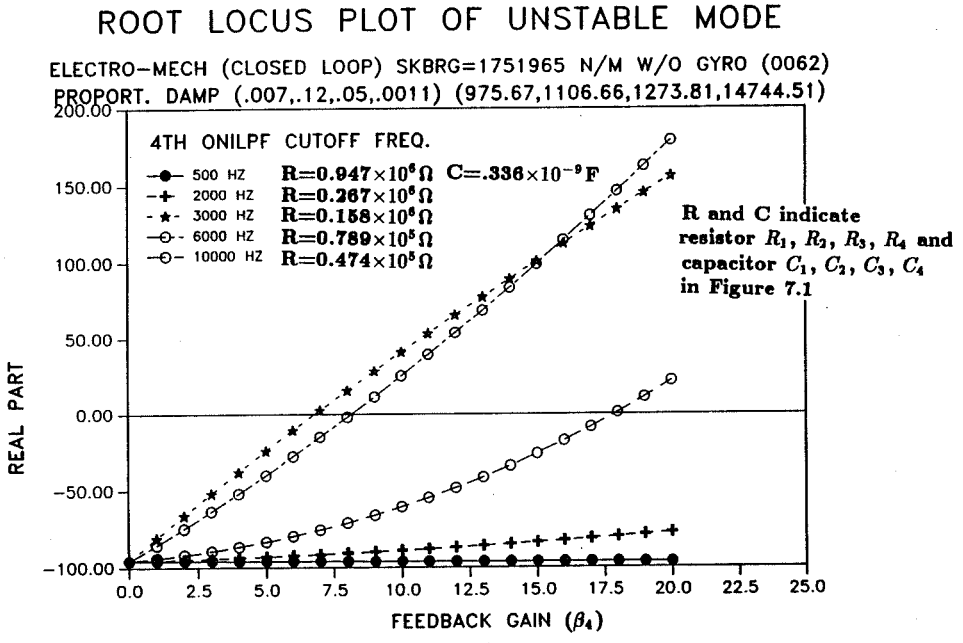

Figure 12 **Effects of cutoff frequency of 4NILPF on the system instability onset gain.**

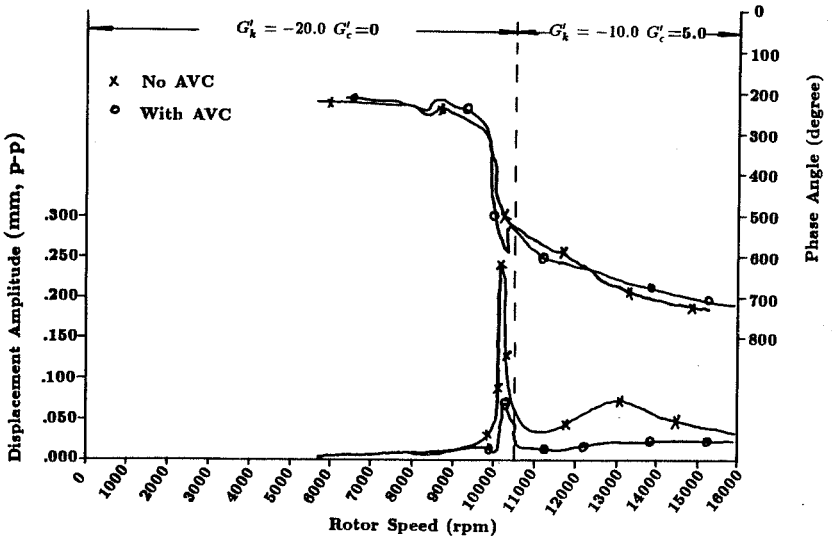

Figure 13 Midspan vibration with and without active damping and stiffness.